3D IMAGING BASED ON SINGLE PHOTON DETECTORS

Cristiano Niclass, Mineki Soga*, and Edoardo Charbon

Ecole Polytechnique Fédérale de Lausanne, CH-1015 Lausanne – Switzerland
*Toyota Motor Europe NV/SA, B-1930 Zaventem – Belgium

KEYWORDS: Geiger-mode avalanche photodiode, SPAD, 3D camera, time-of-flight, TCSPC.

ABSTRACT

This paper introduces a mathematical model to evaluate fast and cost-effective 3D image sensors based on single photon detectors. The model will help engineers evaluate design parameters based on operating conditions and system performance. Ranging is based on the time-of-flight principle using TCSPC techniques. Two scenarios are discussed: (i) short-distance range indoors and (ii) medium-distance range outdoors. The model predicts an accuracy of 0.25cm at 5m with 0.5W of illumination and 1klux of background light. In the medium-range scenario, a precision of 0.5cm is predicted at 50m with 20W of illumination and 20klux of background light.

1. INTRODUCTION

Interest in cost-effective and miniaturized three-dimensional (3D) cameras has grown significantly since the publication of the first solid-state ranging imagers based on CCD/CMOS technologies [1]-[8]. As widely acknowledged in the literature, single-photon detectors (SPD) and, more specifically, single-photon avalanche diodes (SPADs) bring high timing precision to 3D imaging. This paper focuses on the modeling and simulation of solid-state 3D image sensors based on SPADs in standard CMOS technology for two evaluation scenarios: (i) short range up to 7.5m and (ii) medium range up to 50m. The model assumes time-of-flight (TOF) rangefinding using time-correlated single photon counting (TCSPC), as in [5]. The model is based on simple and inexpensive signal processing steps so as to reduce area utilization and power consumption on an integrated solution.

References [9] and [10] present two mathematical models for performance evaluation that can be applied to rangefinders based on SPADs. In both models, it was assumed that SPADs operate in "gated" mode. By definition, in gated mode a sensor is active within a time window. For instance, if the distance of the target is known, gating may reduce the influence of background light by blocking it outside a given interval around the corresponding TOF. This technique is particularly useful for single-shot measurements to reduce the probability that the SPAD is in dead time during the time window of interest due to a background photon. Single-shot measurements are especially attractive when the range of detection is very large, thus reducing the time available for averaging.

In [9], a probabilistic model was developed to assess the probability of correct detection and the probability of false alarms. The model is suitable when the number of averaged illumination pulses is limited to 1-10. However, TCSPC relies on a relatively large number of measurements for histogram processing, allowing excellent noise reduction. The model described in [9] is therefore not used in this work. Reference [10] is also based on gated operation of SPDs. The special case considered by the authors is characterized by means of an artificial photon detection probability exponentially decreasing with respect to TOF. This undesirable behavior only occurs when gating is assumed.

In our model, due to the short distance ranges we deal with, a continuous free-running mode is more appropriate. In free-running mode, the SPD can be triggered at any time. Upon photon absorption, the usual dead time applies. Assuming a dead time lower than the illumination repetition period, the TCSPC principle will not exhibit the artificial behavior of [10]. As a result, the model proposed in [10] is not used in this work for general performance evaluation, except for the estimation of

distortion. In addition, in free-running mode, the total count rate of the SPD can be much higher than the illumination repetition rate.

The model was built so as to make the decision on design parameters easier. Examples of design parameters are illumination power, illumination pulse width, optical SNR, and time-to-digital resolution. In addition, robustness of the distance measurement is also taken as a design parameter.

2. IMAGING PRINCIPLE AND OPERATING CONDITIONS

2.1 Range Imaging Principle

TCSPC is a technique for the measurement of time properties of low light level signals. This technique has been used for many decades in research, especially in particle physics and biology. Fig. 1 shows the principle of a 3D imaging setup based on TCSPC. The method uses a pulsed light source with high repetition rate to illuminate the target. SPDs are used to detect back-reflected photons and to trigger a time-to-digital-converter (TDC), thereby measuring the round-trip TOF of the light beam. TCSPC requires that a relatively large number of detection cycles be collected to build a histogram. The main assumption is that background light (BG) and any intrinsic detector noise (DN) are not correlated to the illuminating pulses. As a result, the contribution of DN and BG is uniformly distributed in the histogram. The signal, by contrast, is correlated to the illumination light and thus generates an accurate replica of the illumination pulse waveform in the histogram. Under certain conditions of signal-to-noise ratio (SNR), BG and DN can be nearly fully separated from the signal. The position of the illumination pulse in the histogram provides TOF. The distance from target to image plane *d* of each imaged point is computed according to the formula shown in the picture, ideally in a parallel fashion.

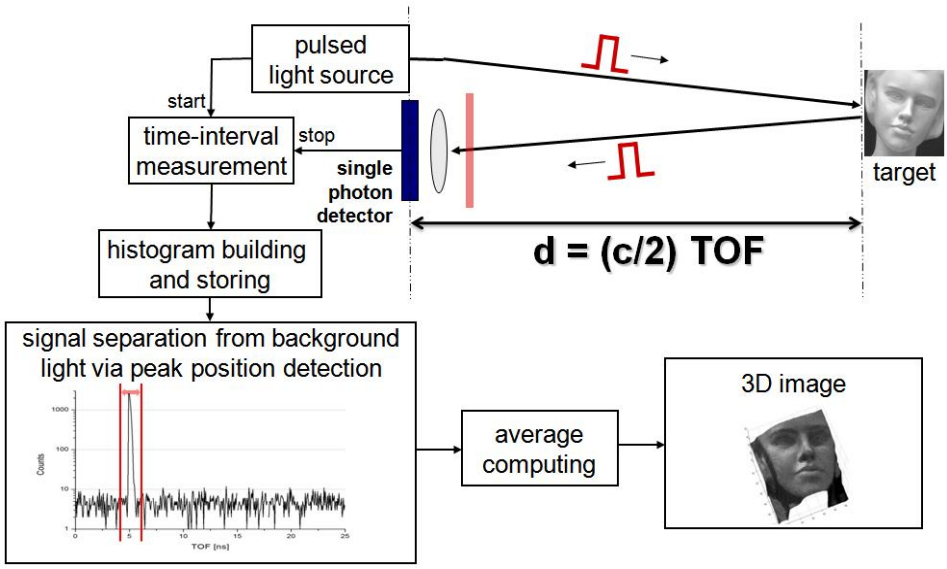

Fig. 1. 3D imaging setup based on TCSPC. The histogram shown here represents a measurement example.

2.2 Background Light

Background light is a major issue for any 3D image sensor operating outdoors. In order to correctly predict the influence of this omnipresent source of noise, we used a simple model based on Planck's Blackbody radiation at a temperature of 6000°C. In this paper, we neglect the presence of attenuation in the atmosphere at certain wavelengths. This simplification remains very reasonable in the very near infrared spectral range, which is the range assumed in this work. The main input parameter for this model is the total illuminance in klux. The illuminance is converted to irradiance, (in W/cm^2), to be used with measurements of photon detection probability. The illuminance considered outdoors is 100klux. Nonetheless, since it corresponds to a normal incidence, a more appropriate value of 20klux is used.

2.3 Optical Component Parameters

In order to reduce the effects of background light on the image plane, a narrow-band interference optical filter (NBOF) is used. NBOFs are commercially available and can be readily customized for a given application. The main parameters of NBOF are (a) the central passband wavelength (λ_0), (b) the passband full width at half maximum (FWHM) in nanometers, (c) the maximum transmission at the passband peak, and (d) the stopband transmission. Though NBOFs with passband FWHM as low as 1nm are commercially available, we prefer to relax this constraint. This choice allows for λ_0 to vary as a function of the incidence angle. It also accounts for active illumination (λ_L) variability due to temperature variations and aging. An additional optical component included in the model is the imaging lens. The imaging lens is simply modeled in terms of its f-number (*f/#*). Tab. 1 lists the operating conditions used in this work.

Tab. 1. List of parameters assumed in this work.

Parameter	Description	(i) Short range	(ii) Med. range	Unity
BG	Total background light illuminance	1	20	klux
α_{FV}	Diagonal field-of-view angle considering a aspect ratio of 1:1	40	25	°
R_D	Maximum target distance (range)	7.5	50	m
f_0	Illumination repetition rate (or cyclic frequency)	20	3	MHz
T_0	Illumination period ($1/f_0$)	50	333.33	ns
IAP	Illumination average power	0.5	20	W
σ_τ	Illumination half pulse width (Gaussian shape, $\sigma_\tau \cong 0.425$FWHM)	0.25	1	ns
Δt	Resolution of time-to-digital converter	50	200	ps
λ_L, λ_0	Illumination and NBOF central wavelength	785		nm
FW	NBOF FWHM in the passband	30		nm
PBT	NBOF peak transmission in the passband	50		%
SBT	NBOF transmission in the stopband	0.01		%
$f/\#$	Imaging lens f-number	f/2.0		m^{-1}
R_O	Target object reflectivity	50		%
F_R	Image frame rate	20		fps
T	Integration time (defined as the inverse of F_R)	1/20		ms
D_{SPAD}	SPAD diameter	10		μm
FF_{SPAD}	SPAD fillfactor	10		%
η, PDP_{SPAD}	SPAD photon detection probability at λ_L	10		%
SAT_{SPAD}	SPAD count rate at saturation	30		MHz
σ_{SPAD}	SPAD timing jitter (RMS)	35		ps

3. TCSPC DETECTION MODELING

Another very important assumption in TCSPC is that, on average, less than a photon from active signal is detected per cycle. When this condition is not met, the signal experiences distortion. This is commonly known as "pile-up" effect in TCSPC. Many authors reported ways to correct pile-up distortions when it is moderate [11]. In order to keep pile-up distortion below reasonable levels, it is possible to intentionally reduce the detector count rate via attenuator or filter as assumed in [9] and [10]. Pile-up distortion may be analytically evaluated by assuming for instance a Gaussian shape for the illumination optical pulse [10], i.e.,

$$P(t) = \frac{Q}{\sqrt{2\pi}\sigma_\tau} \exp\left(-\frac{(t - TOF)^2}{2\sigma_\tau^{\,2}} \right), \tag{1}$$

where Q is the optical energy per illumination pulse, σ_τ characterizes the pulse width, and $P(t)$ is the optical power. Assuming Poisson statistics, the distorted optical power $\tilde{P}(t)$ becomes

$$\tilde{P}(t) = P(t) \exp\left(-\frac{\eta Q}{2} \left(erf\left(-\frac{t}{\sqrt{2}\sigma_\tau} \right) + 1 \right) \right), \tag{2}$$

where η is the photon detection probability (PDP) of the SPD and $erf(\cdot)$ is the *error function* of a normal distribution. If M is the number of photons from active signal detected on average per illumination cycle, then we may find a practical limit to be applied in a 3D image sensor. As an

example, equation (2) may be evaluated for M=1. In this case, the distortion causes a timing error of approximately 20% of the optical pulse width (σ_τ). In practice, depending on desired accuracy, this condition can be assumed as the upper limit for acceptable distortion. When extremely high precision is required, one should consider lower counting rate. Numerical simulations show that when M is 0.1 or below, distortion effects become negligible.

A TCSPC system can be optimized by increasing the illumination repetition rate to the maximum allowed. Let T_0 be the period of the illumination cycle, then for a given measurement distance range R_D, the illumination repetition frequency f_0 can be defined as

$$f_0 = \frac{1}{T_0} = \frac{c}{2R_D}, \tag{3}$$

where c is the speed of light. Since M is a function of target distance and reflectivity, it is difficult to choose a fixed attenuation factor that covers the full range of a 3D image sensor. Practical realizations of this method will make designers opt for a variable and electrically tunable attenuator. If the SPD is implemented as a SPAD, one may vary its PDP as a function of the counting rate in a closed-loop circuit. This circuit may be additionally used to regulate SPAD biasing in large temperature range and could be adjusted to implement this additional function. The actual implementation of the assumed closed-loop attenuation circuit is beyond the scope of this paper.

Assuming a Gaussian illumination pulse as in (1), an average photon detection rate from BG and DN as $\langle N \rangle$, an average photon detection rate from active signal as $\langle S \rangle$, then we can define the optical SNR as

$$SNR = \frac{\langle S \rangle}{\langle N \rangle}. \tag{4}$$

Hence, the total average photon detection rate of a SPD is assumed to be $\langle S \rangle + \langle N \rangle$. When the proposed setup is used to build a histogram during integration time T, the histogram $h^*(\tau)$ can be described by

$$h^*(\tau) = n^*(\tau) + s^*(\tau), \tag{5}$$

where $n^*(\tau)$ and $s^*(\tau)$ are random variables. In order to simplify the notations hereafter, $h^*(\tau)$, $n^*(\tau)$ and $s^*(\tau)$ will be described by their mean values $h(\tau)$, $n(\tau)$, and $s(\tau)$, respectively. Assuming that the resolution of TDC (Δt) is smaller than σ_τ, it follows that $n(\tau)$, the contribution from BG and DN in the TCSPC measurement, is given by

$$n(\tau) = \bar{n} = \frac{\langle N \rangle T}{T_0} \Delta t; \tag{6}$$

$s(\tau)$ describes the signal density in $h(\tau)$ and it has almost the same shape of $P(t)$,

$$s(\tau) = \frac{\langle S \rangle T \cdot \Delta t}{\sqrt{2\pi}\sigma_\tau} \exp\left(-\frac{(\tau - TOF)^2}{2\sigma_\tau^{\,2}} \right), \tag{7}$$

where TOF is the time-of-flight to be measured. Fig. 2 shows the mean value of histogram $h(\tau)$ and a snapshot of $h^*(\tau)$ for a given set of parameters. $h^*(\tau)$ is shown to illustrate the effect of its randomness due to $n^*(\tau)$ and $s^*(\tau)$. One should notice that $h^*(\tau)$ is a discrete function with constant time intervals given by Δt.

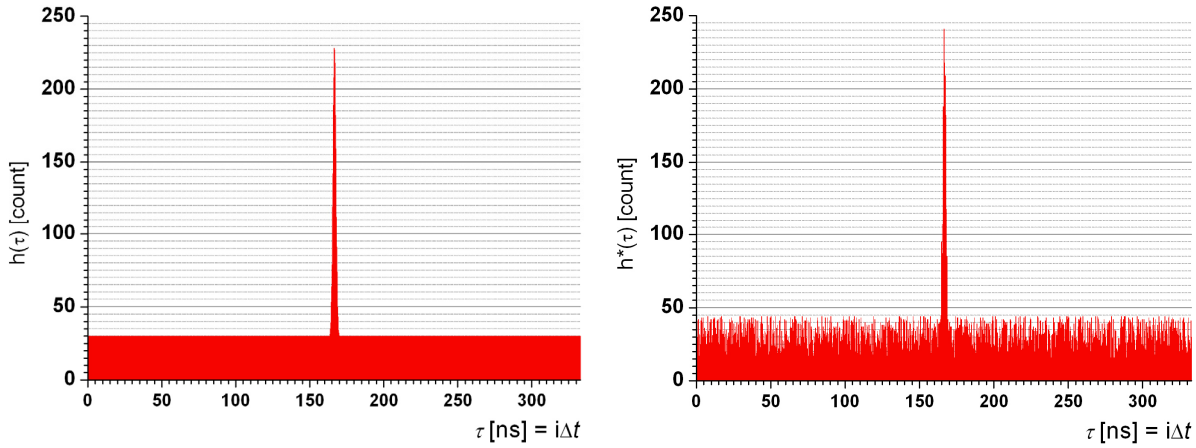

Fig. 2. Histogram mean value $h(\tau)$ (left-hand side) and $h^*(\tau)$ (right-hand side). Assuming SNR = -26dB, T_0 = 333.33ns, σ_τ = 1ns, Δt = 200ps, $\langle N \rangle = 10^6$ Hz, TOF = 166.67ns, T = 50ms.

As seen in Fig. 2, TCSPC enables clear discrimination between signal and noise even at low SNR. Among different algorithms, in this model, we focus on an algorithm that uses the timing position of the signal's peak as a reference to perform noise suppression. This approach has a number of advantages. For instance, the values taken by $h(\tau)$ will vary over a very large range due to measurement conditions such as *SNR* and target's reflectivity, whereas the timing position of the signal's peak for a fixed target does not. Let the timing position of the signal's peak be *TOF'* and its pulse width be *PW*, then one could accurately determine *TOF* very simply as following

$$TOF' = j\Delta t \quad \text{such that} \quad h(j\Delta t) = MAX\{h(k\Delta t)\}, \quad k \in \left[0,1,\cdots,k < \frac{T_0}{\Delta t}\right] \tag{8}$$

then we use the time interval

$$\tau \in \left[TOF' - \frac{PW}{2}, TOF' + \frac{PW}{2}\right] \tag{9}$$

to determine a mean value of τ. The mean value of τ may be estimated as the abscissa of the centroid of $h(\tau)$,

$$TOF = \bar{\tau} = \frac{\sum_{i=TOF'-\frac{PW}{2}}^{TOF'+\frac{PW}{2}} h(i\Delta t)\cdot i\Delta t}{\sum_{i=TOF'-\frac{PW}{2}}^{TOF'+\frac{PW}{2}} h(i\Delta t)}. \tag{10}$$

Note that *PW* is known *a priori* and it does not depend, to a first approximation, on measurement conditions. Indeed, *PW* is the pulse width of the resulting convolution between the overall detection circuit response function and the illumination pulse $P(t)$. *PW* is therefore chosen to accommodate the worst-case spreading of the signal pulse. In addition, *TOF'* can be effortlessly computed during histogram generation using a simple hardware register when fully digital implementation is adopted, thus reducing the post-processing window only to interval given by (9).

Using the proposed algorithm, we can determine the conditions under which one could, with a desired certainty, accurately find TOF'. The computation of TOF' is a crucial step to retrieve the actual TOF value. As can be expected, the probability of an incorrect estimation of TOF' increases when SNR is exceedingly low. Let us assume that one requires a reliable measurement of TOF with a given confidence level stated by a probability *P*. For instance, let us assume the user desires to

rely on 99.7% of the TOF measurements, i.e. P=0.997. Then, we can predict that the signal will be successfully discriminated from noise, by successfully obtaining *TOF'*, when

$$h(TOF') - \alpha_s \sigma_s > \bar{n} + \alpha_n \sigma_n, \tag{11}$$

where σ_s and σ_n are the standard deviations of the quantities $h^*(TOF')$ and $n^*(\tau)$ respectively. α_s and α_n are parameters used to set the confidence level of the measurement given by

$$\alpha_s = \sqrt{2} \cdot erf^{-1}(P), \text{ and} \tag{12}$$

$$\alpha_n = \sqrt{2} \cdot erf^{-1}\left(1 - \frac{(1-P)}{\frac{T_0}{\Delta t} - 1}\right) \cong \sqrt{2} \cdot erf^{-1}\left(1 - \frac{T_0}{\Delta t}(1-P)\right). \tag{13}$$

where $erf^{-1}(\cdot)$ is the *inverse error function*. Assuming that $h^*(TOF')$ and $n^*(\tau)$ are Poisson-distributed, we can determine their standard deviations σ_s and σ_n as

$$\sigma_s = \sqrt{h(TOF')} \text{ and } \sigma_n = \sqrt{\bar{n}}. \tag{14}$$

Based on equations (6)-(7), (11), one can determine the minimum signal count $<S>$ necessary to perform a correct detection with confidence level given by P via

$$< S >_{MIN} = \frac{4\pi \cdot \sigma_\tau^{\,2}}{T \cdot \Delta t} \left(erf^{-1}(P) \sqrt{\frac{1}{\sqrt{2\pi} \cdot \sigma_\tau} + \frac{1}{SNR \cdot T_0}} + \frac{erf^{-1}\left(1 - \frac{\Delta t}{T_0}(1-P)\right)}{\sqrt{SNR \cdot T_0}} \right)^2. \tag{15}$$

$<S>_{MIN}$ may be used to determine the minimum illumination power necessary to ensure a *reliable measurement* using (8) and (10). If this constraint is not met, even though a *TOF* value can be computed, there is no guarantee that it is a reliable measure. It is possible that different algorithms[1] would allow *TOF* to be confidently determined when the condition on $<S>_{MIN}$ is not satisfied. Nonetheless, in this model, we chose an algorithm that is fast, accurate and inexpensive.

Under the condition of equation (15), we can determine the standard deviation of *TOF*, i.e. σ_{TOF}. In particular, we will use the benefits of averaging to improve precision. *TOF* is defined as the centroid position of the light pulse within the interval given by (9). When performing each *TOF* measurement using (10), the fluctuations of $n^*(\tau)$ and $s^*(\tau)$ lead to an uncertainty on *TOF*. Let us assume that there exist two contributions to such uncertainty. Let us also assume that these contributions are two statistically independent random variables with zero mean. Then, the variance of *TOF* can be modeled as a linear combination of $\sigma_{TOF,N}^2$ and $\sigma_{TOF,S}^2$, i.e. the variances due to the fluctuations of $n^*(\tau)$ and $s^*(\tau)$, respectively. Considering that every point of $n^*(\tau)$ within interval (9) is a statistically independent random variable whose mean value is $\bar{n}$ and whose standard deviation is σ_n, then, by applying the formula of error propagation on equation (10) $\sigma_{TOF,N}$ is determined as follows

$$\sigma_{TOF,N} = \Delta t \cdot \sqrt{\frac{\left(\frac{PW}{\Delta t}\right)^2 - 1}{12 \cdot \left(\frac{PW}{\Delta t}\right) \cdot \bar{n} \cdot \Delta t}} = \Delta t \cdot \sqrt{\frac{SNR \cdot T_0 \left(\left(\frac{PW}{\Delta t}\right)^2 - 1\right)}{12 \cdot PW \cdot T \cdot < S >}}. \tag{16}$$

[1] For instance, algorithms based on curve fitting, on scale space filtering, or on bump hunting procedure.

The term $\sigma_{TOF,S}$ is determined by inspection, assuming a reduction of the single-shot error σ_τ by square root of the number of signal measurements stored in $s(\tau)$, i.e.

$$\sigma_{TOF,S} = \frac{\sigma_\tau}{\sqrt{\sum_{k=TOF'-PW/2}^{TOF'+PW/2} s(k \cdot \Delta t)}} = \frac{\sigma_\tau}{\sqrt{< S > \cdot T \cdot erf\left(\frac{PW}{2\sqrt{2}\sigma_\tau}\right)}}. \tag{17}$$

Finally, σ_{TOF} is determined by combining (16) and (17) into σ_{TOF} as

$$\sigma_{TOF} = \frac{1}{\sqrt{< S > \cdot T}} \frac{\sqrt{\frac{PW \cdot \Delta t^2}{12 \cdot SNR \cdot T_0}\left(\left(\frac{PW}{\Delta t}\right)^2 - 1\right) + erf\left(\frac{PW}{2\sqrt{2}\sigma_\tau}\right)\sigma_\tau^2}}{\frac{PW}{SNR \cdot T_0} + erf\left(\frac{PW}{2\sqrt{2}\sigma_\tau}\right)}. \tag{18}$$

In order to evaluate σ_{TOF} as a function of the distance, we introduce an attenuation factor in the model so as to reduce the pile-up effect, i.e.. $< S > + < N > \le f_0$. The attenuation is applied simultaneously on the signal and on BG. As a result, the pile-up effect will be limited as follows

$$M \le \frac{1}{1 + \frac{1}{SNR}}. \tag{19}$$

4. SIMULATION RESULTS

Based on the parameters of Tab. 1 and assuming $PW = 2\sigma_\tau$, we evaluated the performance of TCSPC measurements in the two proposed scenarios. Note that σ_{TOF} is converted to distance uncertainty.

4.1 Short Range Scenario

Fig. 3 shows <S>, <N>, and <S_{MIN}> as a function of target distance. As <S> reduces quadratically with the target distance due to the divergence of the illumination beam (field-of-view angle), the attenuation circuit is active only when the target is extremely close to the camera. The parameters of Tab. 1 for short range are a good compromise between illumination power and distance accuracy. Indeed, <S> is higher than <S_{MIN}> throughout the distance range. The worst-case distance uncertainty is 0.25cm (σ_{TOF} of 16.6ps) whereas the distance resolution is 0.75cm (ΔT of 50ps).

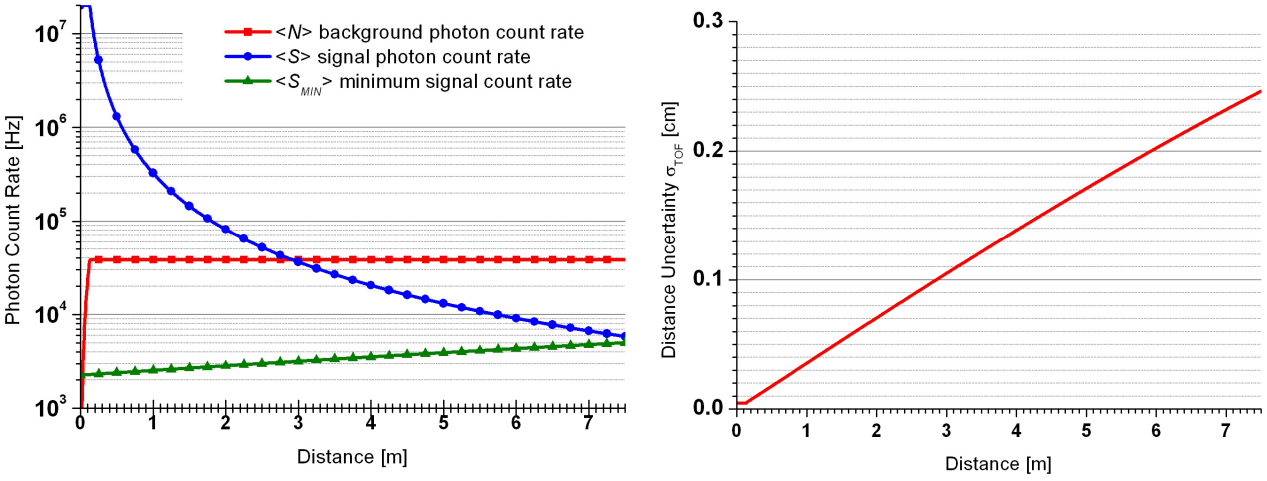

Fig. 3. <S>, <N>, and <S_{MIN}> as a function of target distance for the short range scenario (left). Distance uncertainty σ_{TOF} as a function of target distance (right).

4.2 Medium Range Scenario

Similarly to the previous scenario, Fig. 4 shows <*S*>, <*N*>, and <S_{MIN}> as a function of target distance for the medium range evaluation scenario. The worst-case distance uncertainty is 0.5cm (σ_{TOF} of 33.3ps) whereas the distance resolution is 3cm (ΔT of 200ps).

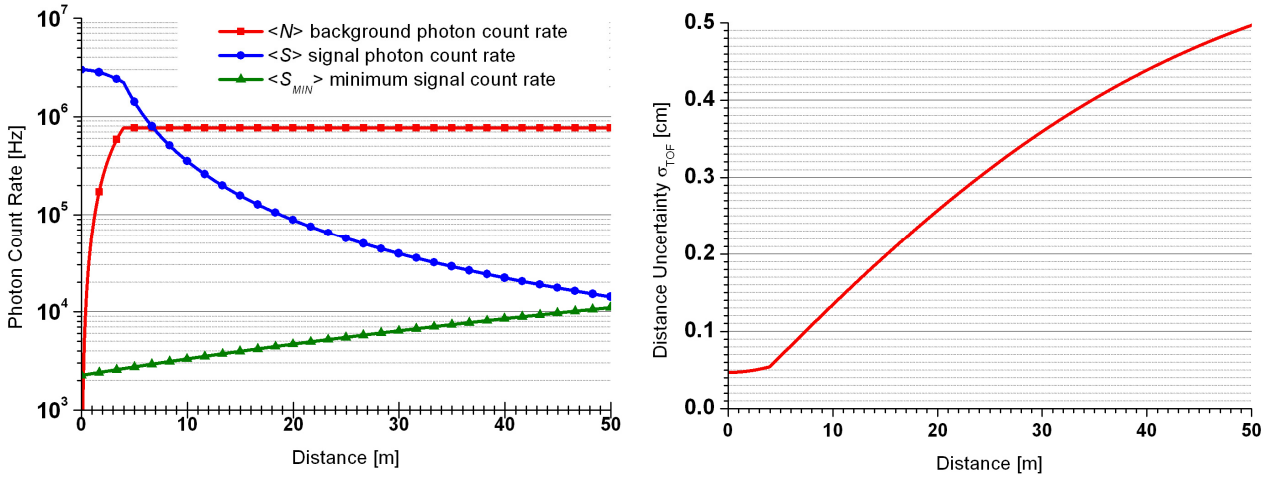

Fig. 4. <*S*>, <*N*>, and <S_{MIN}> as a function of target distance for the medium range scenario (left). Distance uncertainty σ_{TOF} as a function of target distance (right).

5. CONCLUSION AND ACKNOWLEDGEMENTS

A simple model for 3D imagers based on solid-state SPDs and TCSPC was introduced. The model assumes a very simple signal processing on the TCSPC histogram data. Means are presented to compute system design parameters effectively. This research was partially supported by a grant of the Swiss National Science Foundation.

REFERENCES

[1] R. Jeremias et al., "A CMOS Photosensor Array for 3D Imaging Using Pulsed Laser", *Dig. Tech. Papers ISSCC*, pp. 252-253, Feb 2001.

[2] R. Lange and P. Seitz, "Solid-state time-of-flight range camera", *IEEE Journal of Quantum Electronics*, Vol. 37, Issue 3, pp. 390-397, Mar 2001.

[3] R. Schwarte, "Dynamic 3D-Vision", *Int. Symp. on Electron Devices for Microwave and Optoelectronic Applications*, pp. 241-248, Nov 2001.

[4] S.B. Gokturk et al., "A Time-Of-Flight Depth Sensor - System Description, Issues and Solutions", *Computer Vision and Pattern Recognition Workshop*, p. 35, Jun 2004.

[5] C. Niclass and E. Charbon, "A single photon detector array with 64x64 resolution and millimetric depth accuracy for 3D imaging", *Dig. Tech. Papers ISSCC*, pp. 364–365, Feb 2005.

[6] D. Stoppa et al., "Scannerless 3D Imaging Sensors", *Proc. IEEE IST*, pp. 58-61, May 2005.

[7] T. Ushinaga et al., "A QVGA-size CMOS time-of-flight range image sensor with background light charge draining structure", *Proc. SPIE 6056*, Jan 2006.

[8] G. Yahav et al., "3D Imaging Camera for Gaming Application", *Proc. ICCE*, pp.1-2, Jan 2007.

[9] D. G. Fouche, "Detection and false-alarm probabilities for laser radars that use Geiger-mode detectors", *Applied Optics*, Vol. 42, No. 27, 2003.

[10] M. Rohner et al., "Single-Photon Detection for High Precision Ranging – A trade-off Study", *RIM Conference*, ETH Zurich, 2005.

[11] P. B. Coates, "The correction of photon pile-up in the measurement of radiative lifetimes", *J. Sci. Instrum., J. Phys E*, 1, Series 2, pp. 878-879, 1968.